

Solar-Driven Reduction of 1 atm of CO₂ to Formate at 10% Energy-Conversion Efficiency by Use of a TiO₂-Protected III–V Tandem Photoanode in Conjunction with a Bipolar Membrane and a Pd/C Cathode

Xinghao Zhou,^{†,‡} Rui Liu,[‡] Ke Sun,^{‡,§} Yikai Chen,[‡] Erik Verlage,^{†,‡} Sonja A. Francis,^{‡,§,||} Nathan S. Lewis,^{*,‡,§,⊥,#} and Chengxiang Xiang^{*,‡,§}

[†]Division of Engineering and Applied Science, Department of Applied Physics and Materials Science, [‡]Joint Center for Artificial Photosynthesis, [§]Division of Chemistry and Chemical Engineering, ^{||}Resnick Sustainability Institute, [⊥]Beckman Institute and Molecular Materials Research Center, and [#]Kavli Nanoscience Institute, California Institute of Technology, Pasadena, California 91125, United States

Supporting Information

ABSTRACT: A solar-driven CO₂ reduction (CO₂R) cell was constructed, consisting of a tandem GaAs/InGaP/TiO₂/Ni photoanode in 1.0 M KOH(aq) (pH = 13.7) to facilitate the oxygen-evolution reaction (OER), a Pd/C nanoparticle-coated Ti mesh cathode in 2.8 M KHCO₃(aq) (pH = 8.0) to perform the CO₂R reaction, and a bipolar membrane to allow for steady-state operation of the catholyte and anolyte at different bulk pH values. At the operational current density of 8.5 mA cm⁻², in 2.8 M KHCO₃(aq), the cathode exhibited <100 mV overpotential and >94% Faradaic efficiency for the reduction of 1 atm of CO₂(g) to formate. The anode exhibited a 320 ± 7 mV overpotential for the OER in 1.0 M KOH(aq), and the bipolar membrane exhibited ~480 mV voltage loss with minimal product crossovers and >90 and >95% selectivity for protons and hydroxide ions, respectively. The bipolar membrane facilitated coupling between two electrodes and electrolytes, one for the CO₂R reaction and one for the OER, that typically operate at mutually different pH values and produced a lower total cell overvoltage than known single-electrolyte CO₂R systems while exhibiting ~10% solar-to-fuels energy-conversion efficiency.



The sustainable electrochemical reduction of CO₂ requires utilization of CO₂ from the atmosphere as well as use of the electrons and protons produced by the oxidation of water to O₂(g).^{1,2} However, CO₂ reduction (CO₂R) involves very different optimal electrolyte conditions than oxidation of water. For the cathodic CO₂R reaction in alkaline conditions (e.g., pH > 10), the low concentration of dissolved CO₂ imposes severe mass-transport limitations on the electroactive reagent,^{3–5} whereas in acidic conditions (e.g., pH < 1), the high proton concentration favors the competing hydrogen-evolution reaction (HER). Hence, the development of catalysts for CO₂R has generally focused on electrolytes having near-neutral pH values.^{6,7} At present, in near-neutral pH electrolytes, only electrochemical processes that involve the two-electron/two-proton reduction of CO₂, to produce either CO or formate, can be performed efficiently and selectively at an operating current density of 10¹ mA cm⁻².^{6,8–11} In contrast, for the oxygen-evolution reaction (OER), mixed-metal oxides

have been extensively studied in strongly alkaline conditions (1.0 M KOH(aq)), with state-of-the-art catalysts exhibiting ~250–300 mV overpotentials at 10 mA cm⁻² of anodic current density.^{12,13} Electrocatalysts for the OER in near-neutral electrolytes exhibit substantially larger overpotentials than OER electrocatalysts in alkaline electrolytes^{13–15} because the negatively charged hydroxide ion is more readily oxidized than a neutral water molecule, and because hydroxide is present in high concentration in alkaline solutions.¹⁶

Most laboratory demonstrations of solar-driven CO₂R devices have used a single electrolyte at near-neutral pH values but consequently suffer substantial overpotential losses for the OER.^{9,17–19} For example, a 6.5% solar-to-fuel conversion efficiency, η_{STF} , was reported using a Au catalyst for CO

Received: August 2, 2016

Accepted: September 9, 2016

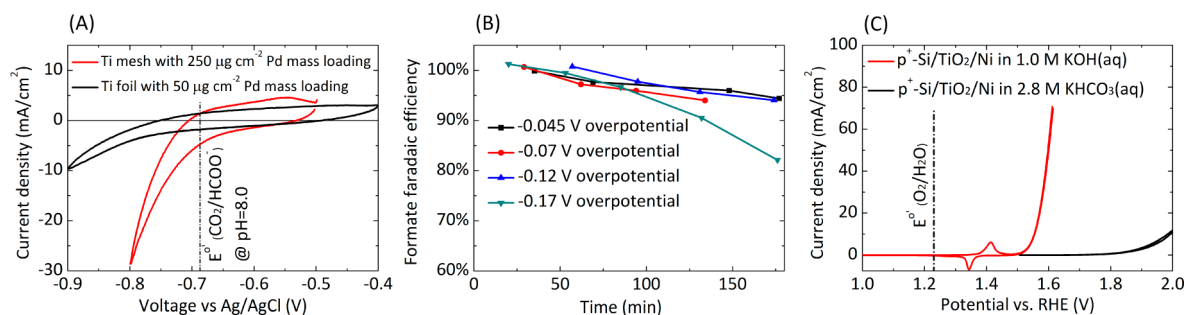


Figure 1. (A) Cyclic voltammetry of the Pd/C nanoparticle-coated stacked Ti mesh electrode with a Pd mass loading of 250 μg cm⁻² (red) and the Pd/C nanoparticle-coated Ti foil with a Pd mass loading of 50 μg cm⁻² (black) in CO₂-saturated 2.8 M KHCO₃(aq) at pH = 8.0. The dotted line indicates the equilibrium potential for CO₂ reduction to formate at pH = 8.0. The three-electrode cell configuration is shown in Figure S2A. (B) Faradaic efficiency of formate production as a function of time, for four different overpotentials, using the Pd/C nanoparticle-coated Ti mesh in CO₂-saturated 2.8 M KHCO₃(aq). (C) Current–potential behavior of a p⁺-Si/TiO₂/Ni electrode for the OER in 1.0 M KOH(aq) (red) and in 2.8 M KHCO₃(aq) (black).

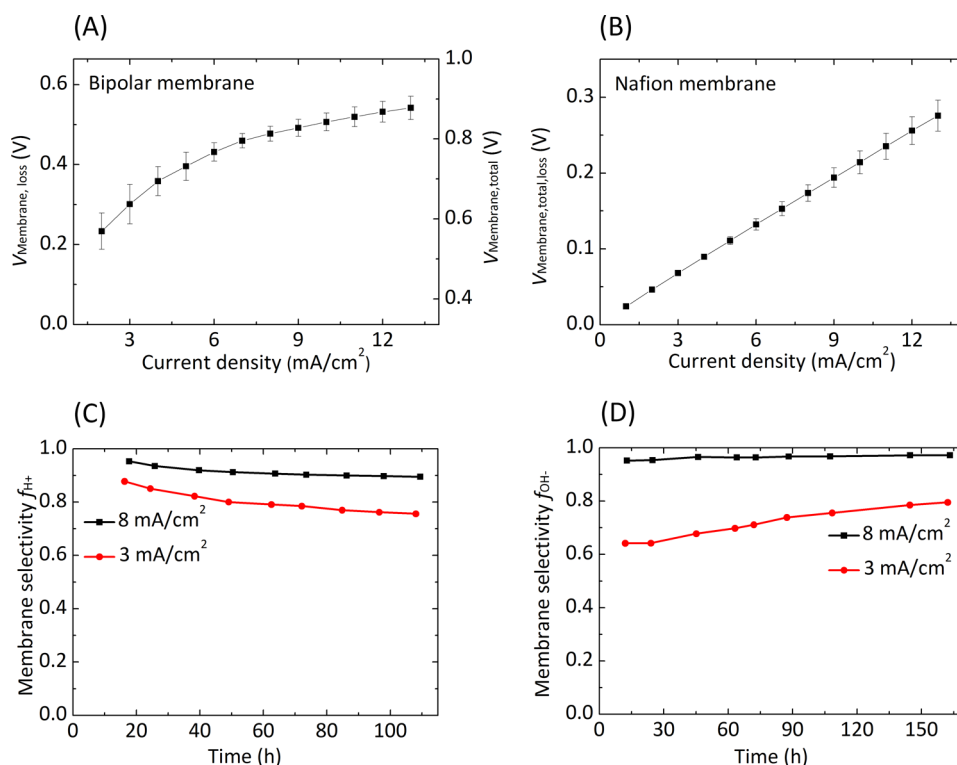


Figure 2. (A) Membrane voltage loss (left axis) and measured total membrane voltage (right axis) as a function of the current density normalized to the 0.03 cm² BPM area. The cell configuration was KHCO₃(aq) (pH = 8.0)/BPM/KOH (aq, pH = 13.7) (Figure S2C). (B) Measured total membrane voltage (or membrane voltage loss) as a function of the current density normalized to the Nafion area. The cell configuration was KHCO₃(aq) (pH = 8.0)/Nafion/KHCO₃(aq) (pH = 8.0) (Figure S2C). (C) Selectivity of the BPM for protons as a function of time, when operated at two different current densities. (D) Selectivity of the BPM for hydroxide ions as a function of time, for two different current densities. Pt mesh electrodes were used as the cathode and anode in (C) and (D).

generation in 0.5 M NaHCO₃(aq) electrolyte.⁹ A value of $\eta_{\text{STF}} = 4.6\%$ was obtained using a polymeric Ru complex for formate generation in 0.1 M aqueous phosphate buffer.¹⁷ In addition to requiring effective ionic coupling between the catholyte and anolyte, a full solar-driven CO₂R system also requires a robust means to separate the products as well as facile collection of the reduced fuels. We demonstrate herein the performance of a photovoltaic-assisted electrosynthetic cell in which the photoanode is operated in 1.0 M KOH(aq) (pH = 13.7) to perform the OER while the cathode performs the CO₂R reaction in 2.8 M KHCO₃(aq) (pH = 8.0) under 1 atm of CO₂(g). The pH difference between the cathode chamber and the anode

chamber was sustained at steady state with no accompanying chemical bias voltage by use of a bipolar membrane (fumasep FBM).^{20–23} Hence, two electrolytes having mutually different pH values, with each electrolyte individually optimized for the CO₂R reaction or the OER, were effectively coupled together to produce a modest combined cell overvoltage at the desired operational current density.

The photoanode (GaAs/InGaP/TiO₂/Ni) consisted of a tandem-junction III–V photoabsorber, an amorphous hole-conductive TiO₂ protection layer, and a thin catalyst layer to facilitate the OER.^{24,25} Details of the fabrication of the photoanode are described in the Supporting Information

(SI). The water-oxidation behavior of the photoanode in 1.0 M KOH(aq) under simulated 1 sun illumination has been characterized previously,²⁴ and the photoanode exhibited a light-limited photocurrent density of $\sim 8.5 \text{ mA cm}^{-2}$ and an equivalent open-circuit voltage of $\sim 2.4 \text{ V}$, (Figure S1), in accord with prior results.^{24,25}

Figure 1A shows the cyclic voltammetry, at a scan rate of 10 mV s^{-1} without correction for uncompensated resistance (see Figure S2A for an illustration of the three-electrode electrochemical measurement setup), of a Pd/C nanoparticle-coated Ti mesh cathode with a Pd mass loading of $250 \mu\text{g cm}^{-2}$ (red) and a Pd/C-coated Ti foil with a Pd mass loading of $50 \mu\text{g cm}^{-2}$ (black) in 2.8 M $\text{KHCO}_3(\text{aq})$ (pH = 8) that was saturated with a stream of 1 atm of $\text{CO}_2(\text{g})$. The Pd/C cathode was fabricated by drop-casting a solution containing 2 mg mL^{-1} Pd/C nanoparticles and $\sim 0.15 \text{ wt } \%$ Nafion in isopropanol on a Ti mesh or a Ti foil. The Pd/C-coated Ti foil (black curve in Figure 1A) exhibited very similar electrocatalytic activity to that reported previously.⁸ The Pd/C-coated stacked Ti mesh electrode exhibited improved performance because of the increased mass loading and larger electrochemically accessible surface area for CO_2R reduction. The forward scan indicated that the onset potential of the cathodic current was close to the equilibrium potential for CO_2 reduction to formate ($E^\circ(\text{CO}_2/\text{HCOO}^-) = -0.687 \text{ V}$ versus the Ag/AgCl reference electrode).²⁶ An overpotential of $-57 \pm 8 \text{ mV}$ was required to drive CO_2R at a cathodic geometric current density of 10 mA cm^{-2} . Figure 1B shows the Faradaic efficiency for the production of formate using the Pd/C nanoparticle-coated Ti mesh cathode in CO_2 -saturated 2.8 M $\text{KHCO}_3(\text{aq})$ as a function of time, at four different overpotentials. At all overpotentials, near-unity Faradaic efficiency was observed for the first 60 min of operation. The Faradaic efficiency then decreased slowly for overpotentials between -45 and -120 mV , but still exceeded $\geq 94\%$ after 3 h of electrolysis (Figure 1B). In contrast, when the electrode was held at -170 mV vs $E^\circ(\text{CO}_2/\text{HCOO}^-)$, the Faradaic efficiency decayed quickly after 90 min and decreased to $\sim 80\%$ after 3 h of continuous operation (see the SI for discussion about the time dependence of the Faradaic efficiency). The decrease of the Faradaic efficiency for formate production is consistent with the accumulation of CO at the surface of the Pd nanoparticles.⁸ To characterize in detail the performance of the protection layer and electrocatalytic components of the anode, Figure 1C shows the current density vs potential (J - E) behavior of a p^+ -Si/TiO₂/Ni dark anode affecting the OER in 1.0 M KOH(aq) (black) and in 2.8 M $\text{KHCO}_3(\text{aq})$ (red) without any correction for uncompensated resistance. The J - E behavior of the p^+ -Si/TiO₂/Ni dark electrode was used to provide a measure of the overpotentials of the OER catalyst in 1.0 M KOH(aq) and in 2.8 M $\text{KHCO}_3(\text{aq})$ (see the SI for discussion of the nickel catalyst). As shown in Figure 1C, an overpotential of $330 \pm 10 \text{ mV}$ was required to produce a current density of 10 mA cm^{-2} in 1.0 M KOH(aq), consistent with previous results.²⁷ In contrast, an overpotential of $793 \pm 26 \text{ mV}$ was required in 2.8 M $\text{KHCO}_3(\text{aq})$ to produce 10 mA cm^{-2} of current density.

With the anolyte at pH = 13.7 (1.0 M KOH(aq)) and the catholyte at pH = 8.0 (2.8 M $\text{KHCO}_3(\text{aq})$), Figure 2A shows the membrane voltage loss (left axis), as well as the measured total membrane voltage (right axis) as a function of the current density normalized to the bipolar membrane (BPM) area (see Figure S2C for an illustration of the four-point measurement configuration).²⁵ Two Luggin capillaries with Ag/AgCl

reference electrodes were used to measure the electric potential drop across the BPM. The equilibrium potential, $V_{\text{membrane, equilibrium}}$ was calculated to be 0.336 V in the anolyte/catholyte system. At a current density of 10 mA cm^{-2} , the measured membrane total voltage was $0.843 \pm 0.038 \text{ V}$. Hence, to drive the reduction of CO_2 to formate at steady state, the voltage loss in the BPM, $V_{\text{membrane, loss}} = V_{\text{membrane, total}} - V_{\text{membrane, equilibrium}} = 0.843 \text{ V} - [0.059 \text{ V} \times (13.7 - 8.0)]$, was 0.507 V. The voltage loss primarily resulted from the resistance loss of the BPM as well as from the overvoltage required for water dissociation at the transition region in the BPM. The observed membrane voltage losses in the 1.0 M KOH(aq) (pH = 13.7)/2.8 M $\text{KHCO}_3(\text{aq})$ (pH = 8.0) system were substantially smaller than those previously reported in 0.5 M $\text{KH}_2\text{BO}_3(\text{aq})$ (pH = 9.3)/1.0 M $\text{H}_2\text{SO}_4(\text{aq})$ (pH = 0)²⁵ because the flexible Luggin capillaries used in the present study were placed very close to the membrane and minimized the resistive losses due to the solution. To evaluate the ionic transport properties of the membrane, a cell with Pt mesh electrodes as the cathode and anode was operated continuously for 100 h at a current density of $\sim 8.5 \text{ mA cm}^{-2}$ normalized to the BPM area, with a resulting change by ~ 0.01 unit in the pH of the anolyte. If 100% of the charge passed had been used for electro dialysis of the electrolytes, the pH of the anolyte would have changed by >1 unit. After continuous operation of this cell for 6 h at 8.5 mA cm^{-2} , the BPM voltage changed by $<0.5\%$ (Figure S3). Alternatively, for operation of CO_2R and OER in the same electrolyte, a cation-exchange membrane, for example, Nafion, could be used to separate the cathode chamber from the anode chamber. Figure 2B shows the measured total membrane voltage as a function of the current density normalized to the Nafion area, when both the anolyte and catholyte were 2.8 M $\text{KHCO}_3(\text{aq})$, but Nafion was used instead of a BPM. The total Nafion membrane voltage was equal to the Nafion membrane voltage loss, which largely arose due to the membrane resistance for transport of K^+ ions. At a current density of 10 mA cm^{-2} , the voltage loss across the Nafion membrane was $214 \pm 15 \text{ mV}$.

The ion-crossover fluxes in the BPM system were characterized using inductively coupled plasma mass spectrometry (ICPMS) in conjunction with a total inorganic carbon (TIC) analyzer to measure the ion concentrations in the catholyte and anolyte after charge was passed through the BPM at different current densities. Figure 2C–D shows the time dependence of the selectivity of the BPM for protons and hydroxide ions at two different operational current densities. Two major crossover pathways, cation crossover from the anolyte to the catholyte and anion crossover from the catholyte to the anolyte, were present under the electric field due to the imperfect permselectivity of the cation-exchange membrane and anion-exchange membrane portions of the BPM. To determine the cation crossover, the $\text{KHCO}_3(\text{aq})$ catholyte was replaced by $\text{CsHCO}_3(\text{aq})$, so that small increases in the K^+ concentration could be detected. The measured K^+ leak rate in the $\text{CsHCO}_3(\text{aq})/\text{KOH}(\text{aq})$ configuration also presented an upper bound for the behavior of the $\text{KHCO}_3(\text{aq})/\text{KOH}(\text{aq})$ configuration due to the absence of the diffusional driving force for K^+ transport from the anolyte to the catholyte in the all- K^+ -containing system. The membrane selectivities, f_{H^+} (f_{OH^-}), were defined as the ratio of proton-carried (hydroxide-carried) charge passed relative to the total charge passed through the membrane. At an operational current density of 3 mA cm^{-2} , the potassium leak current and the bicarbonate leak current

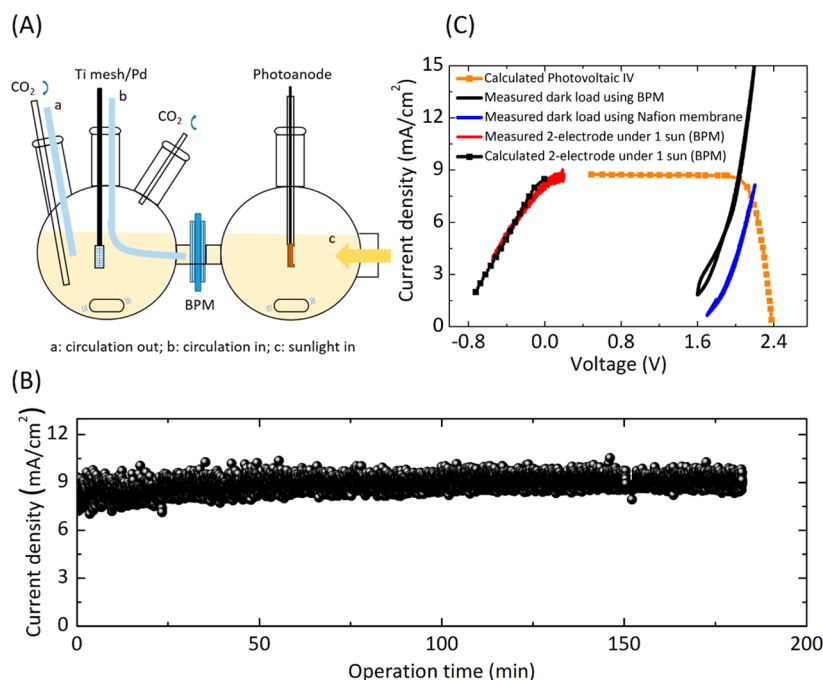


Figure 3. (A) Schematic illustration of a two-electrode electrochemical setup. The blue tubes were connected to a peristaltic pumping system, which facilitated the removal of CO₂ bubbles and prevented voltage loss caused by bubbles. (B) The unassisted CO₂R current density as a function of operational time using a GaAs/InGaP/TiO₂/Ni photoanode and a Pd/C-coated Ti mesh cathode in a two-electrode electrochemical configuration (panel A) under 100 mW cm⁻² of simulated AM1.5 illumination. (C) The overall polarization characteristics for the CO₂R reaction and the OER using a p⁺-Si/TiO₂/Ni anode and a Pd/C-coated Ti mesh cathode in the two-electrode BPM configuration (KHCO₃/Nafion/KOH) (black) as well as in the two-electrode Nafion membrane configuration (KHCO₃/Nafion/KHCO₃) (blue). The measured (red) and calculated (black) two-electrode current–voltage behavior of the GaAs/InGaP/TiO₂/Ni photoanode wired to a Pd/C-coated Ti mesh cathode was measured under 100 mW cm⁻² of simulated AM1.5 illumination. The calculated current density–voltage characteristic of the solid-state tandem cell (orange).^{24,25}

constituted 10–25% and 20–35%, respectively, of the total current passed through the BPM. When the membrane current density was increased to 8 mA cm⁻², the membrane selectivity for protons increased to >90% and the membrane selectivity for hydroxide ions increased to >95%. The crossover of the formate product was low (Figure S4). In the three-electrode electrochemical measurement, the cathode compartment was separated from the Pt counter electrode by a BPM; therefore, the high Faradaic efficiency (>94%) measured in the cathode compartment at low overpotentials (from -45 to -120 mV, Figure 1B) also provides evidence for a low rate of formate crossover through the BPM. The product crossovers were minimal because the negatively charged formate ion was effectively blocked by the negatively charged cation-exchange membrane in the BPM system.

Figure 3A shows a schematic illustration of the two-electrode electrochemical setup. CO₂ at 1 atm (ALPHAGAZ 1) was bubbled continuously into the 2.8 M KHCO₃(aq) catholyte. The blue tubes shown in the figure were connected to a peristaltic pumping system that facilitated removal of CO₂ bubbles and thus minimized associated fluctuations in the cell voltage and current. The geometric areas of the GaAs/InGaP/TiO₂/Ni photoanode, BPM, Nafion membrane, and Pd/C/Ti cathode were mutually similar, at 0.030, 0.030, 0.030, and 0.040 cm², respectively. The relatively small active device area was due to the behavior of the photoanode in 1.0 M KOH(aq). The electrocatalytic performance, stability, and Faradaic efficiency for product formation at the cathode, the *J*–*E* properties of the photoanode, and the current–voltage characteristics of the BPM were independent of the geometric areas of these cell

components (Figure S5), but the stability of the photoanode was dependent on the electrode area due to pinholes and other defects at large electrode areas, providing a source for active dissolution and thus instability of the III–V semiconductors in 1.0 M KOH(aq) (see the SI). Small-area photoanodes have exhibited stable operation for >100 h with near-unity Faradaic efficiency for the OER.^{24,28} Figure 3B shows the current density for unassisted CO₂R as a function of the time under 100 mW cm⁻² of simulated AM1.5 illumination, when the GaAs/InGaP/TiO₂/Ni photoanode was directly wired to the Pd/C nanoparticle-coated Ti mesh cathode without application of any external bias. The photocurrent density was 8.7 ± 0.5 mA cm⁻². The overpotential for the Pd/C nanoparticle-coated Ti mesh cathode was recorded during the 3 h stability test, as shown in Figure S6A. During the stability test, the overpotential was between -40 and -100 mV; therefore, as shown in Figure 1B, the Faradaic efficiency of CO₂ reduction to formate was ~100, 98, 95, and 94% after 30 min, 1 h, 2 h, and 3 h, respectively. The corresponding solar-to formate conversion efficiency at these times was thus 10.5, 10.3, 10.0, and 9.9%, respectively (the see SI for details on calculation of the solar-to-formate conversion efficiency).^{9,29} The photocurrent density vs voltage behavior of the two-electrode system (Figure S6B) exhibited mutually similar onset potentials and light-limited current densities before and after a 3 h stability test (Figure 3B), indicating minimal corrosion of the photoanode over this time period.

Figure 3C shows the measured (red) and calculated (dotted black) two-electrode current density vs voltage behavior of the GaAs/InGaP/TiO₂/Ni photoanode wired to a Pd/C-coated Ti

mesh cathode under 100 mW cm^{-2} of simulated Air Mass (AM)1.5 illumination. The calculated two-electrode current density vs voltage behavior (dotted black) was obtained by using the current–voltage behavior of the tandem solid-state photoabsorber (dotted orange) in conjunction with the overall polarization characteristic of a $\text{p}^+\text{-Si/TiO}_2/\text{Ni}$ anode and a Pd/C-coated Ti mesh cathode in the two-electrode BMP configuration ($\text{KHCO}_3/\text{BPM}/\text{KOH}$) (black). The calculated two-electrode current density vs voltage behavior was in good agreement with the experimental measurements. The electro-synthetic cell component required 2.04 V to operate at a current density of 8.5 mA cm^{-2} and was thus well matched to the maximum power point of the photovoltaic tandem junction component of the photoanode. The electro-synthetic cell thus operated with an electrical-to-fuel conversion efficiency, $\eta_{\text{electrolyzer}}$ of $1.21 \text{ V}/2.04 \text{ V} = 59.3\%$ at 8.5 mA cm^{-2} current density.^{16,29} Figure 3C also shows the overall polarization characteristics of the two-electrode Nafion membrane configuration ($\text{KHCO}_3/\text{Nafion}/\text{KHCO}_3$) (blue) using the same electrode materials. Due to the large overpotential for the Ni catalyst to affect the OER at the near-neutral pH (Figure 1C), obtaining an operational current density of $\sim 8.5 \text{ mA cm}^{-2}$ to drive the overall CO_2R reaction in conjunction with the OER required an additional $\sim 180 \text{ mV}$ of voltage in the Nafion-containing cell relative to the voltage required to operate the BMP-containing cell (Tables S1 and S2). For comparison, a Nafion-containing cell for the electrochemical reduction of 1 atm of CO_2 to CO while performing the OER at the anode in 0.4 M buffered $\text{KH}_2\text{PO}_4(\text{aq})$ (pH = 7.3)/Nafion/0.5 M $\text{KHCO}_3(\text{aq})$ (pH = 7.3) required 2.5 V to produce a current density of 1 mA cm^{-2} .³⁰ Transport of K^+ between the anolyte and catholyte during steady-state operation would also electro-dialyze the electrolytes in the Nafion-containing cell. Circulation or recirculation might potentially minimize the steady-state K^+ ion concentration polarization of the system,³¹ but would entail significant challenges in separation of the low concentration of the liquid product, formate, in the catholyte. In contrast, the robust product separation afforded by the BMP would allow for production of a high concentration of formate, which would be advantageous in a downstream separation process. Additionally, the Ni catalyst is not stable for OER at near-neutral pH.³² Use of the BMP thus relaxed the electrolyte constraints and allowed the incorporation of this active OER catalyst³³ in the device.

TiO_2 -protected tandem III–V photoanodes have been used in a variety of cell configurations to construct high (>10%) efficiency solar-driven water-splitting cells.^{24,25} The J – E performance of the cathodes in such systems³⁴ are comparable to the J – E performance of the Pd/C nanoparticle-coated CO_2R cathodes used herein, providing a basis for comparison of the efficiency losses in each of the cell types in the limit of having a low overpotential, selective cathode in each system. Although the 10% efficiency for CO_2R reported herein is comparable in magnitude to the 10% efficiency reported for photoelectrosynthetic solar-driven water-splitting cells that use either anion exchange or BMPs,^{24,25,35} the efficiencies of these different electro-synthetic cells cannot be directly compared at the system level. Solar-driven water-splitting cells in alkaline electrolytes produce physically separate streams of $\text{H}_2(\text{g})$ and $\text{O}_2(\text{g})$ (either at 1 atm or under higher pressures due to electrochemical compression) from an abundant reagent (including liquid or vapor H_2O from humidified ambient air),^{36,37} have minimal (<100 mV) voltage losses associated with the anion-exchange

membrane and electrolyte, utilize relatively low (<300 mV) overpotential electrocatalysts for the OER, and thus will provide the highest η_{STF} .^{24,38} Use of a BPM allows for operation of the photoanode in electrolytes at near-neutral pH values, which are less corrosive to photoelectrodes, especially for III–V compound semiconductors, relative to the alkaline electrolyte (e.g., 1.0 M KOH), and facilitates the use of relatively large area ($\sim 1 \text{ cm}^2$) photoelectrodes due to stabilization by TiO_2 protective coatings.²⁵ However, BMPs introduce additional membrane-derived voltage losses.^{20–23,25} The near-neutral pH operation also entails increased overpotential losses due to the reduced activity of available OER catalysts operating under such conditions.^{13,32,39,40} The available OER catalysts also obscure light and are semisoluble and unstable on the electrode surface during operation at near-neutral pH.³² In addition, the finite ion crossovers in such cells would eventually lead to electro-dialysis of the electrolyte during passive, long-term cell operation. The CO_2R cells evaluated herein share the same η_{STF} limitations as solar-driven water-splitting systems that utilize a BPM having one electrolyte at near-neutral pH and the other electrolyte under either strongly alkaline or acidic conditions (Tables S1 and S2). The CO_2R cells moreover require that concentrated, purified (to eliminate highly electroactive, ambient O_2) CO_2 feeds are distributed over large electrode areas due to mass-transport limitations on the atmospheric CO_2 flux into aqueous electrolytes,⁵ and they also entail a loss of selectivity in reduction of CO_2 relative to H_2 production at atmospheric (400 ppmv) concentrations of CO_2 in the cathode feed. The formate would also have to be separated from the aqueous solution, as would any other water-soluble CO_2R product such as methanol, ethanol, or isopropanol, requiring an energy-intensive separation step. Use of flue gas as the (unsustainable) CO_2 source would require removal of the electroactive $\text{O}_2(\text{g})$ as well as purification of the flue-gas stream to remove NO_x , SO_x , Hg, and other trace flue-gas components that are either electroactive or that can poison the cathode. The gas stream would then need to be humidified and cooled to near-ambient temperatures, and the resulting gas feedstock distributed over the $\sim 10^7 \text{ m}^2$ area would be required to collect the incident solar photon flux necessary to reduce the CO_2 that is emitted from a 100 MW (electric) coal-fired power plant (see the SI for calculation details). Large storage reservoirs for the CO_2 would also be required to compensate for the 20% capacity factor of the solar-driven photoelectrosynthetic cell relative to the nearly continuous CO_2 emissions stream emanating from the power plant.

In summary, a solar-driven CO_2 reduction photovoltaic-assisted electro-synthetic cell was demonstrated at a solar-to-fuel energy-conversion efficiency of 10% using a tandem GaAs/InGaP/ $\text{TiO}_2/\text{NiO}_x$ photoanode in 1.0 M KOH(aq), a Pd/C nanoparticle-coated Ti mesh cathode in 2.8 M $\text{KHCO}_3(\text{aq})$, and a BPM reducing a purified feed stream of 1 atm of $\text{CO}_2(\text{g})$. At the operational current density of 8.5 mA cm^{-2} , the cathode exhibited <100 mV overpotential and >94% Faradaic efficiency for CO_2 reduction to formate in 2.8 M $\text{KHCO}_3(\text{aq})$ (pH = 8.0), the anode exhibited a $320 \pm 7 \text{ mV}$ overpotential for OER in 1.0 M KOH (aq) (pH = 13.7), and the BPM exhibited a $\sim 480 \text{ mV}$ voltage loss with minimal product crossovers and >90 and >95% selectivity for proton and hydroxide ions, respectively. The BPM effectively coupled together two electrolytes that were separately effective for the CO_2R reaction and for the OER and produced lower total overpotentials and

higher efficiency than could at present be obtained in a single-electrolyte CO₂ reduction cell. The photoelectrosynthetic cells also allowed a comparative evaluation of the operational constraints associated with sustainable solar-driven CO₂ reduction systems relative to sustainable solar-driven water-splitting systems.

■ ASSOCIATED CONTENT

📄 Supporting Information

The Supporting Information is available free of charge on the ACS Publications website at DOI: [10.1021/acseenergylett.6b00317](https://doi.org/10.1021/acseenergylett.6b00317).

Experimental details; calculation details; bipolar membrane and two-electrode configuration (Pd/C-coated Ti mesh/BPM/GaAs/InGaP/TiO₂/Ni) stability data; voltage loss comparison for three cell configurations; low formate crossover data; Faradaic efficiency data for large-area Pd/C-coated Ti mesh cathode; and large-area bipolar membrane voltage loss data (PDF)

■ AUTHOR INFORMATION

Corresponding Authors

*E-mail: nslewis@caltech.edu (N.S.L.).

*E-mail: cxx@caltech.edu (C.X.).

Notes

The authors declare no competing financial interest.

■ ACKNOWLEDGMENTS

This material is based on work performed by the Joint Center for Artificial Photosynthesis, a DOE Energy Innovation Hub, supported through the Office of Science of the U.S. Department of Energy under Award Number DE-SC0004993. S.A.F. acknowledges the Resnick Sustainability Institute at Caltech for a Postdoctoral Fellowship. The authors also thank N. Dalleska (Caltech) for his assistance with measurements and analysis of the ICPMS and TIC data.

■ REFERENCES

- (1) Lewis, N. S.; Crabtree, G.; Nozik, A. J.; Wasielewski, M. R.; Alivisatos, P.; Kung, H.; Tsao, J.; Chandler, E.; Walukiewicz, W.; Spitzer, M.; et al. *Basic Research Needs for Solar Energy Utilization. Report of the Basic Energy Sciences Workshop on Solar Energy Utilization*. Office of Science, U. S. Department of Energy: Washington, DC, 2005.
- (2) Lewis, N. S. Research opportunities to advance solar energy utilization. *Science* **2016**, *351*, aad1920.
- (3) Gupta, N.; Gattrell, M.; MacDougall, B. Calculation for the cathode surface concentrations in the electrochemical reduction of CO₂ in KHCO₃ solutions. *J. Appl. Electrochem.* **2006**, *36*, 161–172.
- (4) Singh, M. R.; Clark, E. L.; Bell, A. T. Effects of electrolyte, catalyst, and membrane composition and operating conditions on the performance of solar-driven electrochemical reduction of carbon dioxide. *Phys. Chem. Chem. Phys.* **2015**, *17*, 18924–18936.
- (5) Chen, Y.; Lewis, N. S.; Xiang, C. Operational constraints and strategies for systems to effect the sustainable, solar-driven reduction of atmospheric CO₂. *Energy Environ. Sci.* **2015**, *8*, 3663–3674.
- (6) Kumar, B.; Llorente, M.; Froehlich, J.; Dang, T.; Sathrum, A.; Kubiak, C. P. Photochemical and Photoelectrochemical Reduction of CO₂. *Annu. Rev. Phys. Chem.* **2012**, *63*, 541–569.
- (7) Hori, Y.; Wakebe, H.; Tsukamoto, T.; Koga, O. Electrocatalytic Process of CO Selectivity in Electrochemical Reduction of CO₂ at Metal-Electrodes in Aqueous-Media. *Electrochim. Acta* **1994**, *39*, 1833–1839.
- (8) Min, X.; Kanan, M. W. Pd-Catalyzed Electrohydrogenation of Carbon Dioxide to Formate: High Mass Activity at Low Overpotential and Identification of the Deactivation Pathway. *J. Am. Chem. Soc.* **2015**, *137*, 4701–4708.
- (9) Schreier, M.; Curvat, L.; Giordano, F.; Steier, L.; Abate, A.; Zakeeruddin, S. M.; Luo, J.; Mayer, M. T.; Gratzel, M. Efficient photosynthesis of carbon monoxide from CO₂ using perovskite photovoltaics. *Nat. Commun.* **2015**, *6*, 7326.
- (10) Asadi, M.; Kumar, B.; Behranginia, A.; Rosen, B. A.; Baskin, A.; Repnin, N.; Pisasale, D.; Phillips, P.; Zhu, W.; Haasch, R.; et al. Robust carbon dioxide reduction on molybdenum disulfide edges. *Nat. Commun.* **2014**, *5*, 4470.
- (11) Asadi, M.; Kim, K.; Liu, C.; Addepalli, A. V.; Abbasi, P.; Yasaei, P.; Phillips, P.; Behranginia, A.; Cerrato, J. M.; Haasch, R.; et al. Nanostructured transition metal dichalcogenide electrocatalysts for CO₂ reduction in ionic liquid. *Science* **2016**, *353*, 467–470.
- (12) Zhang, B.; Zheng, X. L.; Voznyy, O.; Comin, R.; Bajdich, M.; Garcia-Melchor, M.; Han, L. L.; Xu, J. X.; Liu, M.; Zheng, L. R.; et al. Homogeneously dispersed multimetal oxygen-evolving catalysts. *Science* **2016**, *352*, 333–337.
- (13) McCrory, C. C. L.; Jung, S. H.; Peters, J. C.; Jaramillo, T. F. Benchmarking Heterogeneous Electrocatalysts for the Oxygen Evolution Reaction. *J. Am. Chem. Soc.* **2013**, *135*, 16977–16987.
- (14) McCrory, C. C. L.; Jung, S.; Ferrer, I. M.; Chatman, S. M.; Peters, J. C.; Jaramillo, T. F. Benchmarking Hydrogen Evolving Reaction and Oxygen Evolving Reaction Electrocatalysts for Solar Water Splitting Devices. *J. Am. Chem. Soc.* **2015**, *137*, 4347–4357.
- (15) Bockris, J. O. M.; Reddy, A. K.; Gamboa-Aldeco, M. E. *Modern Electrochemistry*; Springer: New York, 2000.
- (16) Xiang, C.; Papadantonakis, K. M.; Lewis, N. S. Principles and implementations of electrolysis systems for water splitting. *Mater. Horiz.* **2016**, *3*, 169–173.
- (17) Arai, T.; Sato, S.; Morikawa, T. A monolithic device for CO₂ photoreduction to generate liquid organic substances in a single-compartment reactor. *Energy Environ. Sci.* **2015**, *8*, 1998–2002.
- (18) Jeon, H. S.; Koh, J. H.; Park, S. J.; Jee, M. S.; Ko, D. H.; Hwang, Y. J.; Min, B. K. A monolithic and standalone solar-fuel device having comparable efficiency to photosynthesis in nature. *J. Mater. Chem. A* **2015**, *3*, 5835–5842.
- (19) Sugano, Y.; Ono, A.; Kitagawa, R.; Tamura, J.; Yamagiwa, M.; Kudo, Y.; Tsutsumi, E.; Mikoshiba, S. Crucial role of sustainable liquid junction potential for solar-to-carbon monoxide conversion by a photovoltaic photoelectrochemical system. *RSC Adv.* **2015**, *5*, 54246–54252.
- (20) Vargas-Barbosa, N. M.; Geise, G. M.; Hickner, M. A.; Mallouk, T. E. Assessing the Utility of Bipolar Membranes for use in Photoelectrochemical Water-Splitting Cells. *ChemSusChem* **2014**, *7*, 3017–3020.
- (21) McDonald, M. B.; Ardo, S.; Lewis, N. S.; Freund, M. S. Use of Bipolar Membranes for Maintaining Steady-State pH Gradients in Membrane-Supported, Solar-Driven Water Splitting. *ChemSusChem* **2014**, *7*, 3021–3027.
- (22) Ünlü, M.; Zhou, J.; Kohl, P. A. Hybrid Anion and Proton Exchange Membrane Fuel Cells. *J. Phys. Chem. C* **2009**, *113*, 11416–11423.
- (23) Vermaas, D. A.; Sassenburg, M.; Smith, W. A. Photo-assisted water splitting with bipolar membrane induced pH gradients for practical solar fuel devices. *J. Mater. Chem. A* **2015**, *3*, 19556–19562.
- (24) Verlage, E.; Hu, S.; Liu, R.; Jones, R. J. R.; Sun, K.; Xiang, C.; Lewis, N. S.; Atwater, H. A. A monolithically integrated, intrinsically safe, 10% efficient, solar-driven water-splitting system based on active, stable earth-abundant electrocatalysts in conjunction with tandem III-V light absorbers protected by amorphous TiO₂ films. *Energy Environ. Sci.* **2015**, *8*, 3166–3172.
- (25) Sun, K.; Liu, R.; Chen, Y.; Verlage, E.; Lewis, N. S.; Xiang, C. A Stabilized, Intrinsically Safe, 10% Efficient, Solar-Driven Water-Splitting Cell Incorporating Earth-Abundant Electrocatalysts with Steady-State pH Gradients and Product Separation Enabled by a Bipolar Membrane. *Adv. Energy Mater.* **2016**, *6*, 1600379.
- (26) Kortlever, R.; Peters, I.; Koper, S.; Koper, M. T. M. Electrochemical CO₂ Reduction to Formic Acid at Low Overpotential

and with High Faradaic Efficiency on Carbon-Supported Bimetallic Pd–Pt Nanoparticles. *ACS Catal.* **2015**, *5*, 3916–3923.

(27) Sun, K.; Saadi, F. H.; Lichterman, M. F.; Hale, W. G.; Wang, H.-P.; Zhou, X.; Plymale, N. T.; Omelchenko, S. T.; He, J.-H.; Papadantonakis, K. M.; et al. Stable solar-driven oxidation of water by semiconducting photoanodes protected by transparent catalytic nickel oxide films. *Proc. Natl. Acad. Sci. U. S. A.* **2015**, *112*, 3612–3617.

(28) Hu, S.; Shaner, M. R.; Beardslee, J. A.; Lichterman, M.; Brunenschwig, B. S.; Lewis, N. S. Amorphous TiO₂ coatings stabilize Si, GaAs, and GaP photoanodes for efficient water oxidation. *Science* **2014**, *344*, 1005–1009.

(29) Coridan, R. H.; Nielander, A. C.; Francis, S. A.; McDowell, M. T.; Dix, V.; Chatman, S. M.; Lewis, N. S. Methods for comparing the performance of energy-conversion systems for use in solar fuels and solar electricity generation. *Energy Environ. Sci.* **2015**, *8*, 2886–2901.

(30) Tatin, A.; Comminges, C.; Kokoh, B.; Costentin, C.; Robert, M.; Savéant, J.-M. Efficient electrolyzer for CO₂ splitting in neutral water using earth-abundant materials. *Proc. Natl. Acad. Sci. U. S. A.* **2016**, *113*, 5526–5529.

(31) Modestino, M. A.; Walczak, K. A.; Berger, A.; Evans, C. M.; Haussener, S.; Koval, C.; Newman, J. S.; Ager, J. W.; Segalman, R. A. Robust production of purified H₂ in a stable, self-regulating, and continuously operating solar fuel generator. *Energy Environ. Sci.* **2014**, *7*, 297–301.

(32) Minguzzi, A.; Fan, F.-R. F.; Vertova, A.; Rondinini, S.; Bard, A. J. Dynamic potential-pH diagrams application to electrocatalysts for water oxidation. *Chem. Sci.* **2012**, *3*, 217–229.

(33) Trotochaud, L.; Young, S. L.; Ranney, J. K.; Boettcher, S. W. Nickel–Iron Oxyhydroxide Oxygen-Evolution Electrocatalysts: The Role of Intentional and Incidental Iron Incorporation. *J. Am. Chem. Soc.* **2014**, *136*, 6744–6753.

(34) Saadi, F. H.; Carim, A. I.; Verlage, E.; Hemminger, J. C.; Lewis, N. S.; Soriaga, M. P. CoP as an Acid-Stable Active Electrocatalyst for the Hydrogen-Evolution Reaction: Electrochemical Synthesis, Interfacial Characterization and Performance Evaluation. *J. Phys. Chem. C* **2014**, *118*, 29294–29300.

(35) Luo, J.; Vermaas, D. A.; Bi, D.; Hagfeldt, A.; Smith, W. A.; Grätzel, M. Bipolar Membrane-Assisted Solar Water Splitting in Optimal pH. *Adv. Energy Mater.* **2016**, *6*, 1600100.

(36) Kumari, S.; Turner White, R.; Kumar, B.; Spurgeon, J. M. Solar hydrogen production from seawater vapor electrolysis. *Energy Environ. Sci.* **2016**, *9*, 1725–1733.

(37) Spurgeon, J. M.; Lewis, N. S. Proton exchange membrane electrolysis sustained by water vapor. *Energy Environ. Sci.* **2011**, *4*, 2993–2998.

(38) Chen, Y.; Hu, S.; Xiang, C.; Lewis, N. S. A sensitivity analysis to assess the relative importance of improvements in electrocatalysts, light absorbers, and system geometry on the efficiency of solar-fuels generators. *Energy Environ. Sci.* **2015**, *8*, 876–886.

(39) Surendranath, Y.; Dincă, M.; Nocera, D. G. Electrolyte-Dependent Electrosynthesis and Activity of Cobalt-Based Water Oxidation Catalysts. *J. Am. Chem. Soc.* **2009**, *131*, 2615–2620.

(40) Kanan, M. W.; Nocera, D. G. In Situ Formation of an Oxygen-Evolving Catalyst in Neutral Water Containing Phosphate and Co²⁺. *Science* **2008**, *321*, 1072–1075.